A Universal Method of Producing Transparent Electrodes Using Wide-Bandgap Materials

*Hee-Dong Kim, Ho-Myoung An, Kyoung Heon Kim, Su Jin Kim, Chi Sun Kim, Jaehee Cho, E. Fred Schubert, and Tae Geun Kim**

A UV light-emitting diode (LED) is an eco-friendly optical source with diverse applications. However, currently, the external quantum efficiency (EQE) of AlGaN-based UV LEDs, particularly in the UV-C band (<280 nm), is very low (<11%) mainly due to a large optical absorption via *p*-GaN contact layers. A direct Ohmic contact to *p*-AlGaN layers should be obtained using UV-transparent conductive electrodes (TCEs) to solve this problem. A universal method is presented here to make such contact using electrical breakdown, with wide-bandgap materials, to form conductive filaments (CFs), providing a current path between the TCEs and the *p*-(Al)GaN layers. The contact resistance between the TCEs and the *p*-GaN layers (or *p*-AlGaN) is found to be on the order of 10^{-5} Ω cm^2 (or 10^{-3} Ω cm^2), while optical transmittance is maintained up to 95% for AlN-based TCEs at 250 nm. These findings could be a critical turning point delivering a breakthrough in UV LED technologies.

1. Introduction

Indium-doped tin oxides (ITOs) have been widely used as transparent conductive electrodes (TCEs) for various types of optoelectronic devices, including light-emitting diodes (LEDs), organic LEDs, and solar cells, that operate in the visible (VIS)-to-infrared (IR) light wave bands (>400 nm).[1–5] However, directly applying the ITO films to optoelectronic devices operating in the ultraviolet (UV) A to C regimes (200–400 nm) is quite challenging because of their large light absorption; the bandgap of ITOs is ~3.4 eV, which fundamentally produces a cut-off wavelength of 365 nm.[6,7] In particular, UV-C LEDs operating at shorter wavelengths (<280 nm) are of special interest, because UV light with a wavelength of 254 nm or less is highly effective in killing microbes. However, AlGaN-based UV-C LEDs require higher aluminum compositions in both the contact and the active layers. This makes it difficult to obtain Ohmic contact between the TCEs and the *p*-GaN (or *p*-AlGaN) layers with high optical transmittance in the UV regimes, eventually resulting in low external quantum efficiency (EQE).[8–14]

Basically, to achieve a highly desirable quantum jump in the deep UV LED technologies, a new method must be developed to form direct Ohmic contacts to the *p*-AlGaN layers with low contact resistance and high transmittance in the UV-C regime. However, with the conventional methods, it is almost impossible to form direct Ohmic contacts to the *p*-AlGaN layers because of the large work-function difference between the metals and the *p*-(Al)GaN layers and the difficulties in increasing doping concentration in the *p*-(Al)GaN layers. In addition to the Ohmic contact issues, it is equally important to achieve high transmittance in the UV regions to minimize light absorption via electrodes using wide-bandgap materials as TCEs. However, if such materials as oxide and nitride groups with bandgap energy (E_g) of over 5.6 eV are used as *p*-type TCEs to increase the transmittance, the conductivity of the TCEs would become extremely low because of the trade-offs between the electrical conductivity and optical transmittance.[15,16]

To provide a fundamental solution to these problems, we present a novel method for achieving both high electrical conductivity and high optical transmittance in the UV A to C regimes by introducing the electrical breakdown (EBD) (or forming) process into the wide-bandgap materials.

2. Results and Discussion

Figure 1a shows the schematic drawing of an AlGaN-based UV LED after EBD, where the zoom-in figure shows that conductive filaments (CFs) can be formed via oxygen or nitrogen vacancies within the TCEs to provide a current path between the TCEs and the *p*-AlGaN layers. To form the CFs within the TCEs, we applied relatively large bias voltages (~17.5 V) to the two metal pads on the TCEs using the Keithley 4200 semiconductor parameter analyzer (SPA). More specifically, we first mechanically connected two nickel electrodes on the TCE using

Dr. H.-D. Kim, H.-M. An, K. H. Kim, S. J. Kim, Prof. T. G. Kim
School of Electrical Engineering
Korea University
Anam-dong 5-ga, Seongbuk-gu, Seoul, 136–701, Korea
E-mail: tgkim1@korea.ac.kr
Dr. C. S. Kim
Materals & Components Lab.
LG Advanced Research Institute
LG Electronics, Baumoe-ro 38, Seocho-gu, Seoul, 137–724, Republic of Korea
Prof. J. Cho, E. F. Schubert
Department of Electrical
Computer, and Systems Engineering
Rensselaer Polytechnic Institute
Troy, NY, 12180, USA

DOI: 10.1002/adfm.201301697

© 2013 WILEY-VCH Verlag GmbH & Co. KGaA, Weinheim

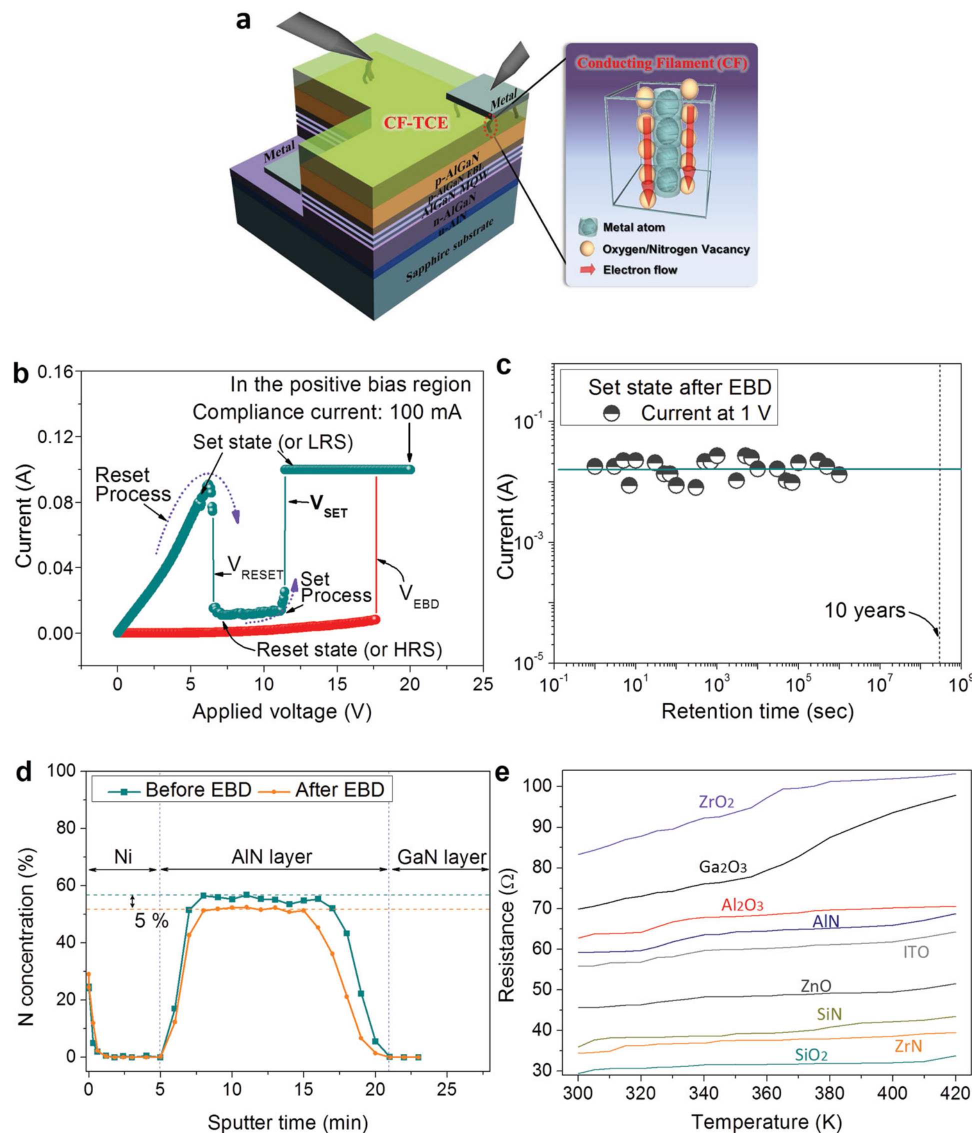

Figure 1. Conduction mechanism and its evidence for the proposed TCEs. a) Artist's view of the AlGaN-based UV LED after EBD, where the zoom-in figure shows that CFs can be formed within the TCEs. b) Current–voltage characteristic curves measured for an 80-nm-thick AlN TCE before and after EBD. c) Retention characteristics of the set state at 1 V as a function of the retention time. d) Nitrogen concentration of the AlN films and the interface between the AlN TCE and the *p*-GaN layer before and after EBD, analyzed by Auger electron spectroscopy. e) Temperature-dependent resistance characteristics of the ITO, Al_2O_3, ZnO, Ga_2O_3, ZrO_2, SiO_2, ZrN, SiN, and AlN TCEs after EBD in the temperature range of 300–420 K.

Keithley 4200 SPA, and applied forward biases from 0 V to 20 V in a current–voltage (*I*–*V*) sweep mode to find a condition for EBD. Then, we swept the voltage again from 0 V to 20 V to check if the CF is formed within the TCE after EBD by observing the linear increase of current level from the *I*–*V* curve. The details of the CF fabrication steps are shown in Figures S1 and S2 of the Supplementary Information. In this experiment, various types of insulators consisting of the oxide and nitride groups (i.e., ZrN, ZnO, ITO, Ga_2O_3, SiN, ZrO_2, AlN, Al_2O_3, and SiO_2) were investigated to gather more general information on the electrical and optical properties of the proposed TCEs for the UV LEDs.

Next, we describe the process of making the wide-bandgap materials conductive (or metallic) using EBD. Figure 1b shows the *I*–*V* characteristic curves with a compliance current of 100 mA, measured under a DC voltage sweep from 0–20 V on a Ni/AlN/*p*-GaN structure at room temperature. Initially, the sample remained in the high resistance state (HRS). However, following the EBD process with electrical voltages from 0–20 V, a sudden increase in the current was observed at ~17.5 V (V_{EBD}) with a current compliance of 100 mA (red line). The sample was thereby switched to the low resistance state (LRS). As the voltage was then re-swept from 0–20 V (cobalt blue line), the current level abruptly increased until the sample was switched back to the HRS at ~6.5 V. The HRS was maintained up to ~12 V and again switched back to the LRS above 12 V. This EBD behavior was also observed under reverse biases in the same manner, as shown in Figure S4a. This phenomenon can

© 2013 WILEY-VCH Verlag GmbH & Co. KGaA, Weinheim

be explained by a soft breakdown process (Supplementary Section SI), often observed in resistance change memory materials.[17–22] The V_{EBD} (or V_{SET}/V_{RESET}) can be adjusted, if necessary, by changing the thickness and composition of the AlN TCE films. Under these conditions, to confirm the availability of the CFs in increasing the conductivity of the AlN TCEs, we first measured the current level at the set state (or LRS), which revealed that the current level increased from a few nanoamperes to ~18 mA and attained the LRS when a voltage of 1 V was applied, as shown in Figure 1b. To examine the long-term stability at the LRS, we then measured the retention characteristics at 1 V in terms of the read delay time, as shown in Figure 1c. The results of this measurement revealed that the low-resistant set state could be maintained for $>10^6$ s. We also extrapolated the result against the read delay time to predict the long-term retention of the sample, and we confirmed that a current level of ~18 mA could be stably maintained for 3×10^8 s (~10 years) at room temperature. On the other hand, considering typical operating voltages of GaN-based UV LEDs,[15] we investigated the electrical stability of the CF-based AlN TCEs under stress biases (V_{ST}) of 3–5 V in pulse height and 1–1000 s in pulse width, as shown in Figures S4b and S4c, and confirmed that the initial set-state current (~18 mA) at 1 V was well maintained even after the application of pulse biases of 3 V/1000 s, 4 V/1000 s, and 5 V/1000 s.

To understand the phenomenon of the abrupt change in resistance, we then investigated the change in atomic concentration in the TCE films using Auger electron spectroscopy analysis before and after the EBD process, as shown in Figure 1d and Figures S5a–S5i. Figure 1d shows the nitrogen concentration of the AlN films before and after EBD. Compared with the TCE films before EBD, the nitrogen concentration decreased on an average by ~5% after EBD. Furthermore, the nitrogen concentration near the interface between the TCEs and the *p*-GaN layers was reduced more prominently. This observation indicates that the CFs might have been formed during the EBD process by the creation of nitride (or oxygen) vacancies in the TCEs, similar to the case of resistance change memory,[17–20] particularly near the *p*-GaN surface, which facilitated the formation of Ohmic contact between the TCEs and the *p*-GaN layers. This result agrees well with the oxygen-mapping result observed by the electron energy-loss spectroscopy and transmission electron microscopy analyses after the EBD.[21,22]

We also examined the temperature-dependent resistance properties to demonstrate the metallic behavior of the proposed TCEs after EBD process. Figure 1e shows the resistance as a function of temperature in the range from 300 K to 420 K, measured for all the TCE samples. This result indicates that the resistance at the set state after EBD process increased with an increase in temperature, similar to the typical electronic transport observed in conductive materials.[22–24]

Next, to examine the contact ability of the CF-based TCEs on the *p*-GaN wafer, we first measured the *I*–*V* characteristic curves of the ZrN, ZnO, ITO, Ga_2O_3, SiN, ZrO_2, AlN, Al_2O_3, and SiO_2 films deposited on the *p*-GaN layers before and after EBD, as shown in **Figures 2**a and b, respectively. Before EBD, the non-linear *I*–*V* characteristics at the current levels of $\sim 10^{-9}$ A at 1 V for all samples were attributed to the large

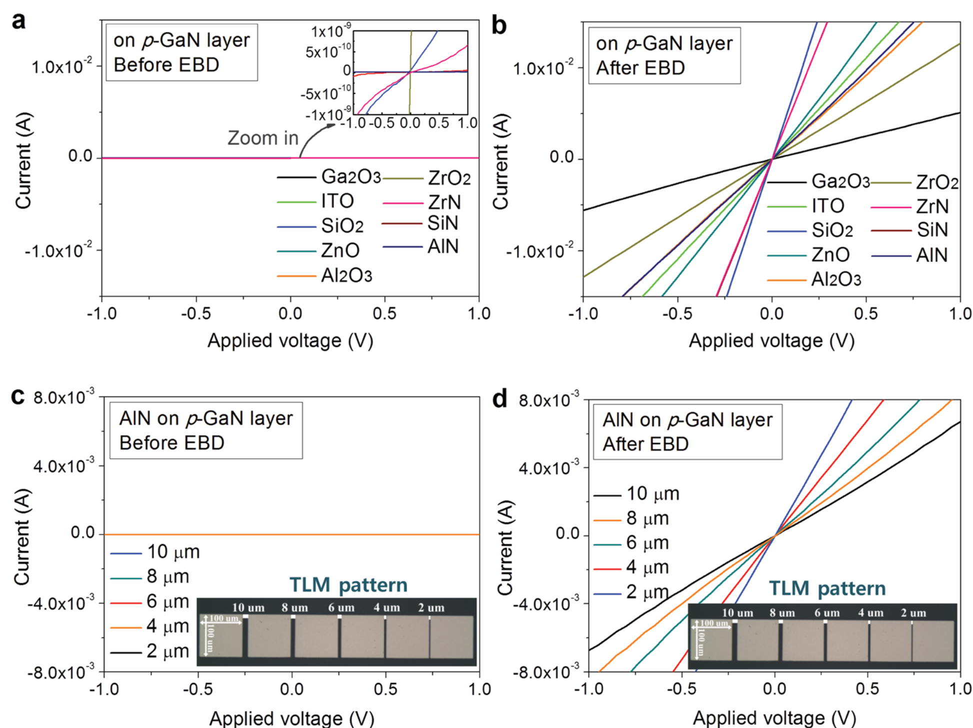

Figure 2. Ohmic behavior of the proposed TCEs on *p*-GaN layers before and after EBD. Typical *I*–*V* characteristic curves measured from ITO, Al_2O_3, ZnO, Ga_2O_3, ZrO_2, SiO_2, ZrN, SiN, and AlN TCEs deposited on *p*-GaN layers a) before and b) after EBD. Each of the plots was measured for the 2-µm-gap metal pads. Typical *I*–*V* characteristic curves measured for the different TLM spacing of the AlN TCEs deposited on *p*-GaN layers c) before and d) after the EBD process at room temperature. The inset figure shows an optical microscope image of the linear TLM pattern for the ρ_c measurement.

© 2013 WILEY-VCH Verlag GmbH & Co. KGaA, Weinheim

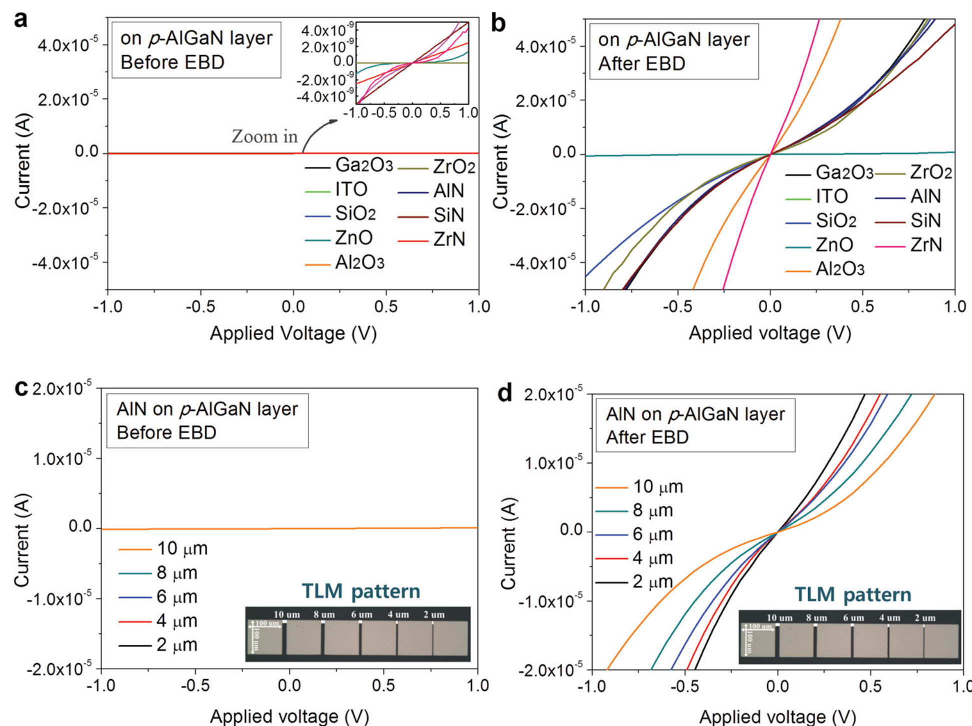

Figure 3. Ohmic behavior of the proposed TCEs on *p*-AlGaN layers before and after EBD. Typical *I–V* characteristic curves measured from ITO, Al_2O_3, ZnO, Ga_2O_3, ZrO_2, SiO_2, ZrN, SiN, and AlN films deposited on *p*-$Al_{0.5}Ga_{0.5}N$ layers a) before and b) after EBD. Each of the plots was measured for the 2-μm-gap metal pads. Typical *I–V* characteristic curves measured for the different TLM spacing of the AlN TCEs deposited on *p*-$Al_{0.5}Ga_{0.5}N$ layers c) before and d) after EBD at room temperature. The inset figure shows an optical microscope image of the linear TLM pattern for the ρ_c measurement.

Schottky barrier height (SBH) between the TCE and the *p*-GaN layer, as well as the extremely low conductivity of the TCEs. However, after EBD, all CF-based TCEs deposited on the *p*-GaN wafer surprisingly showed perfect Ohmic behaviors at current levels of ~10^{-2} A at 1 V in the *I–V* characteristic curve, as shown in Figure 2b. Each of the plots was measured for the 2-μm-gap metal pads.

We also measured the specific contact resistance (ρ_c) of the ZrN, ZnO, ITO, Ga_2O_3, SiN, ZrO_2, AlN, Al_2O_3, and SiO_2 films deposited on the *p*-GaN layers by the linear transfer length method (TLM). The inset in Figure 2c shows an optical microscope image of the linear TLM pattern obtained at the surface of the AlN film with the CFs.[25–27] Figures 2c and d show the typical *I–V* characteristic curves measured for the different TLM spacing of the AlN film contacts before and after EBD at room temperature. After EBD, the AlN-based TCEs with CFs show perfect, linear *I–V* characteristics with Ohmic behavior, where we can deduce the total resistance between any two neighboring contact pads.

Then, we examined the contact ability of the proposed CF-based TCEs on the *p*-$Al_{0.5}Ga_{0.5}N$ wafer, which has never been tried yet because of technical barriers such as the *p*-AlGaN surface oxidation, extremely low Mg doping concentration, and large work function of the *p*-AlGaN, to extend their usage to the deep UV regimes. In the present technology, the *p*-GaN capping layers are inevitably grown on *p*-AlGaN for the Ohmic contact in the AlGaN-based deep UV LEDs because it is difficult to increase the hole concentration of the AlGaN, due to the relatively deep acceptor level of the Mg atoms. However, in this case, most UV light emitted from the AlGaN-based multiple quantum well (MQW) layers is absorbed via the *p*-GaN contact layers, resulting in an extremely low EQE (5–11%). **Figures 3**a and b show the *I–V* characteristic curves measured for the ZrN, ZnO, ITO, Ga_2O_3, SiN, ZrO_2, AlN, Al_2O_3, and SiO_2 films deposited on the *p*-$Al_{0.5}Ga_{0.5}N$ contact layers before and after EBD. Before the EBD, non-Ohmic properties were observed at current levels of ~5 nA at 1 V for all samples, as shown in Figure 3a. However, after EBD, the current levels increased for all CF-based TCEs on the *p*-$Al_{0.5}Ga_{0.5}N$ wafer, and they showed linear (or sub-linear) *I–V* characteristic curves at current levels of over ~10^{-4} A at 1 V, as shown in Figure 3b. Each of the plots was measured for the 2-μm-gap metal pads.

We also measured the ρ_c of the TCE films deposited on the *p*-$Al_{0.5}Ga_{0.5}N$ layers by TLM, as shown in Figures 3c–d and Figures S14–S21. Figures 3c and d show the typical *I–V* characteristic curves measured for different TLM spacing of the AlN film contacts before and after EBD process at room temperature. The AlN-based TCEs with CFs showed sub-linear *I–V* characteristics after EBD, from which we can determine the total resistance between two neighboring contact pads. For the other materials, we also observed improved linearity and increased current levels from tens of picoamperes to tens of microamperes after EBD process. In particular, in the case of the Al_2O_3-based TCEs, the current at 1 V was measured to be over 0.3 mA.

© 2013 WILEY-VCH Verlag GmbH & Co. KGaA, Weinheim

Table 1. Average specific contact resistance, ρ_c, measured between the TCEs and the *p*-GaN layers, calculated from Figures 2c–d and Figures S6–S13, and between the TCEs and *p*-AlGaN layers, calculated from Figures 3c–d and Figures S14–S21, respectively.

Materials [E_g]	Average specific contact resistance, ρ_c [$\Omega \cdot cm^2$]			
	on *p*-GaN layer		on *p*-AlGaN layer	
	Before EBD	After EBD	Before EBD	After EBD
ZrN [2.8 eV]	Non-Ohmic	4.91×10^{-5}	Non-Ohmic	Non-Ohmic
ZnO [3.1 eV]	Non-Ohmic	2.81×10^{-5}	Non-Ohmic	Non-Ohmic
ITO [3.8 eV]	Non-Ohmic	8.68×10^{-5}	Non-Ohmic	Non-Ohmic
Ga_2O_3 [4.8 eV]	Non-Ohmic	7.56×10^{-5}	Non-Ohmic	2.42×10^{-2}
SiN [5.6 eV]	Non-Ohmic	1.01×10^{-5}	Non-Ohmic	2.55×10^{-2}
ZrO_2 [5.8 eV]	Non-Ohmic	4.79×10^{-4}	Non-Ohmic	2.75×10^{-1}
AlN [6.2 eV]	Non-Ohmic	2.41×10^{-5}	Non-Ohmic	4.55×10^{-3}
Al_2O_3 [7 eV]	Non-Ohmic	5.67×10^{-5}	Non-Ohmic	7.10×10^{-3}
SiO_2 [8.9 eV]	Non-Ohmic	1.99×10^{-5}	Non-Ohmic	4.55×10^{-3}

Table 1 shows the average ρ_c measured for the proposed TCEs deposited on the *p*-GaN (left) and *p*-AlGaN layers (right) before and after EBD from six different TLM sets in each sample. The average ρ_c between the CF-based TCEs and the *p*-GaN layers was on the order of ~10^{-5} $\Omega \cdot cm^2$ for all samples, as shown in Figure S22a. These values are comparable with (or lower than) the best result reported from the metal-based *p*-GaN electrodes,[28–30] with the additional benefit of high transmittance of over 95% at 365 nm. For the ρ_c between the CF-based TCEs and the *p*-$Al_{0.5}Ga_{0.5}N$ layers, we observed acceptable values of ρ_c (~10^{-3} $\Omega \cdot cm^2$ on average) for the AlN, Al_2O_3, SiO_2 films, as shown in Figure S22b. However, for the ZrN, ZnO, and ITO films with relatively lower E_g below ~3.4 eV, although the current levels increased by more than 10^3 times compared with those before EBD, we observed Schottky-like behavior in the *I–V* characteristic curves, as shown in Figures S13b–S15b, respectively. These results can be explained by the role of the CFs formed within the TCEs and near the CF-based TCEs/*p*-type (Al)GaN interface. As schematically shown in Figure 1a, the electrons/holes can be injected to the *p*-$Al_{0.5}Ga_{0.5}N$ surface across the TCEs via the CFs and then further injected into the *p*-$Al_{0.5}Ga_{0.5}N$ layers using a vacancy (or defect)-assisted carrier tunneling effect. Because the electrons/holes can be easily transported between the TCEs and the *p*-$Al_{0.5}Ga_{0.5}N$ layers via the CFs (not via the field emission through the thin potential barrier), conventional Ohmic conditions should not be necessarily satisfied; we can possibly achieve Ohmic contact between the TCEs and the lightly doped *p*-AlGaN layers even if the work function of the TCEs is smaller than that of the *p*-AlGaN. Furthermore, the relatively large amount of oxygen or nitride vacancies generated near the CF-based TCEs/*p*-type (Al)GaN interface after EBD process (shown in Figure 1d and Figures S5a–S5h) increases the carrier density at the interface, which leads to the formation of a thin degenerated layer (like delta doping) near the *p*-AlGaN surface and eventually facilitates carrier injection or Ohmic contact formation. Although a perfect Ohmic behavior similar to that observed in the *p*-GaN layers has not been obtained yet for the *p*-AlGaN contact layers (probably because of the still immature technology of the heavily doped *p*-AlGaN layers), the obtained result is not only a first-time demonstration of the direct Ohmic contacts in the *p*-$Al_{0.5}Ga_{0.5}N$ layers but also a critical turning point in delivering a technical breakthrough in the deep UV LED.

On the other hand, to quantitatively evaluate the transparency of the proposed CF-based TCEs, we measured the optical transmittance as a function of the wavelength in the ZrN, ZnO, ITO, Ga_2O_3, SiN, ZrO_2, AlN, Al_2O_3, and SiO_2 films deposited on quartz substrates, as shown in **Figures 4**a and b. From the photograph of the samples placed against the background logo in Figure 4a, we can confirm the very high transmission rates even with a naked eye. The optical transmittance of the TCEs, including the quartz substrate, is measured to be ~95%, on an average, in the deep UV-to-IR wavelength regimes (220–800 nm) for all samples, except for the ITO (3.4 eV), ZnO (3.1 eV), and ZrN (2.8 eV) films because of the bandgap limit of these materials. In particular, for the SiN (5.6 eV), ZrO_2 (5.8 eV), AlN (6.2 eV), Al_2O_3 (8.7 eV), and SiO_2 (8.9 eV) films with a E_g of over ~5.6 eV, we observed a very high transmittance of over 95% at a wavelength of 220 nm.

Finally, we summarize the relationship between the transmittance and the ρ_c with respect to the E_g of each material. **Figure 5** shows the transmittance measured at 250 nm for the various TCE materials with different E_g deposited on the quartz substrates (Figures 5a and b) and the ρ_c measured for the Ohmic contacts between the TCEs and the *p*-GaN layers (Figure 5a) and between the TCEs and the *p*-$Al_{0.5}Ga_{0.5}N$ layers (Figure 5b). First, the transmittance of the TCEs is basically determined by the fundamental E_g of each material. For instance, as far as the UV bands are concerned, the ITO-based TCEs with a E_g of 3.4 eV can cover the UV A regime of 365–400 nm, whereas the SiO_2-based TCEs with a E_g of 8.9 eV can cover the UV B to C regimes of 140–365 nm. That is, the wider the bandgap of the materials we choose, the deeper are the UV bands that we can utilize. Second, the overall ρ_c also depends on the E_g of the TCEs used in this study. In the proposed Ohmic method, to obtain Ohmic contact between the TCEs and the *p*-type semiconductors with a large E_g, such as *p*-AlGaN (7.5 eV), it is advised to use the TCE materials with a E_g of larger than (or similar to) the *p*-type semiconductor, so more electrons/holes could be easily moved from the semiconductors to the TCEs, or vice versa, via the CFs formed

© 2013 WILEY-VCH Verlag GmbH & Co. KGaA, Weinheim

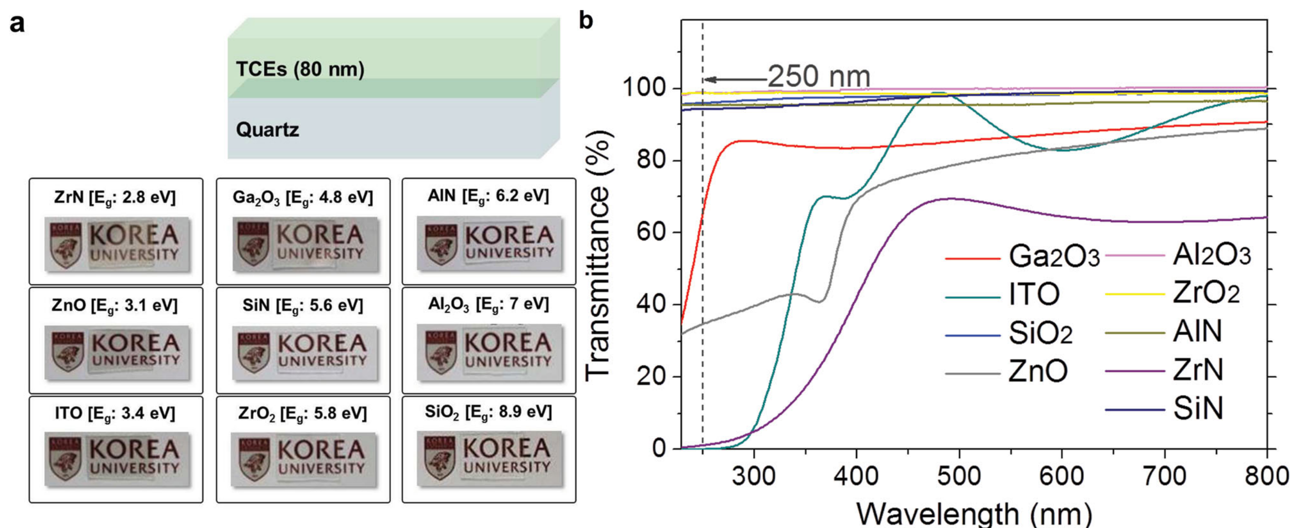

Figure 4. Optical transmittance of the proposed TCEs after EBD. a) Photograph of each sample placed onto a background logo. The upper figure shows the structure for taking photographs. b) Optical transmission spectra measured for the proposed TCEs deposited on quartz substrates in wavelength ranges of 230–800 nm.

within the TCEs and at the TCEs/semiconductor interface. At this condition, Ohmic contact can be easily achieved although the conventional work function condition φ for Ohmic contact ($\varphi_{metal} > \varphi_{semiconductor}$) is not perfectly satisfied. Therefore, we highly expect that the proposed CF-based TCEs can be immediately applied to many types of optoelectronic devices (and systems), including LEDs, organic LEDs, solar cells, and even large-area display panels that require TCEs with high conductivity and high transmittance in the UV-to-IR wavelength regimes.

3. Conclusions

In this article, we present a universal method of producing transparent electrodes with high conductivity and high optical transmittance in the UV regimes using electrical breakdown to form conducting filaments (CFs) providing a current path between the TCEs and the semiconductor, which leads to a large reduction in their contact resistance. As a result, we found the contact resistance between the TCEs and the *p*-GaN layers (or *p*-AlGaN layers) to be on the order of 10^{-5} $\Omega \cdot cm^2$ (or 10^{-3} $\Omega \cdot cm^2$) while optical transmittance is maintained at up to 95% for the AlN-based TCEs at 250 nm. We believe that this result is not only a first-time demonstration of direct Ohmic contacts to *p*-$Al_{0.5}Ga_{0.5}N$ layers but also a critical turning point in delivering a technical breakthrough for deep UV LED technologies (as well as wherever conventional ITO is used.)

4. Experimental Section

Wafer Preparation for Ohmic Contact to p-GaN Layers: UV LED structures with an emission wavelength of 380 nm were grown by

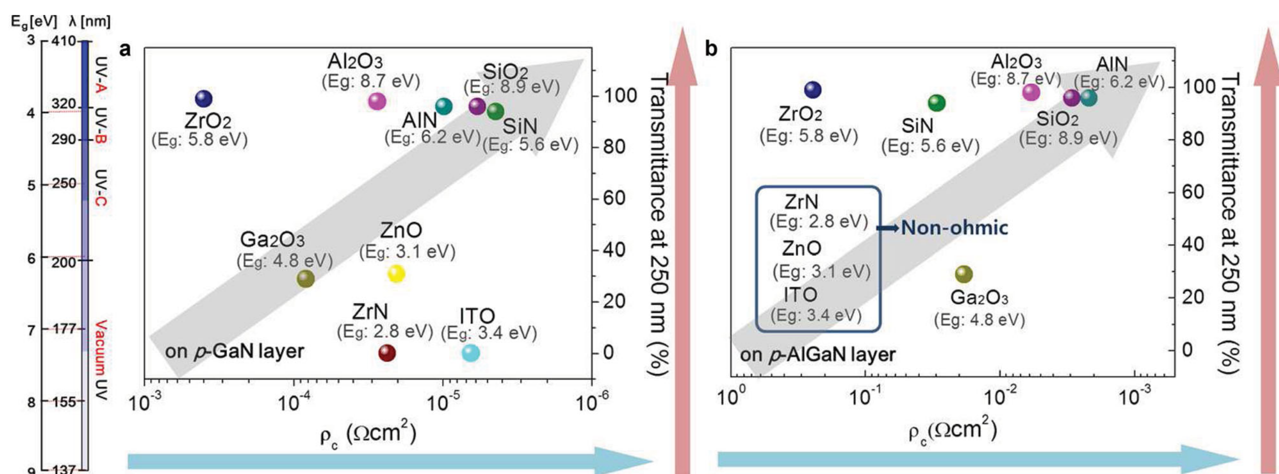

Figure 5. Correlation between the contact resistance, ρ_c, and transmittance at 250 nm measured for the proposed TCEs after EBD. The measurement was done on both (a) the *p*-GaN and (b) the *p*-$Al_{0.5}Ga_{0.5}N$ layers.

© 2013 WILEY-VCH Verlag GmbH & Co. KGaA, Weinheim

metal organic chemical vapor deposition (MOCVD) on a c-plane sapphire substrate. As shown in Figure S1, the LED structures consist of a low-temperature GaN buffer layer, a 2-μm-thick undoped GaN layer, a 3-μm-thick Si-doped *n*-type GaN layer followed by a 0.1-μm-thick $In_{0.03}Al_{0.16}Ga_{0.81}N/In_{0.3}Ga_{0.7}N$ MQW with five periods, a 10-nm-thick *p*-$Al_{0.2}Ga_{0.8}N$ layer, and a 0.2-μm-thick Mg-doped *p*-type GaN contact (or capping) layer. In this sample, a hole concentration of 1×10^{19} cm^{-3} was designed to be achieved after thermal annealing of the *p*-GaN layer.

Wafer Preparation for Direct Ohmic Contact to p-$Al_{0.5}Ga_{0.5}N$ Layers: UV LED structures with an emission wavelength of 280 nm were grown by MOCVD on a buffer layer which consists of 20-nm-thick low-temperature (~700 °C) AlN buffer layer and a 350-nm thick high-temperature AlN layer, as shown in Figure S2. For the epitaxial layers, a 1.8-μm-thick n^+-$Al_{0.6}Ga_{0.4}N$ layer was first grown on the buffer layer to form an *n*-type contact layer with a Si concentration of 2×10^{19} cm^{-3}. Then, the active region consisted of a 7-nm-thick $Al_{0.45}Ga_{0.55}N$ barrier, after which 3.5-nm-thick $Al_{0.42}Ga_{0.58}N$ QWs with six periods were grown, ending with a second 8-nm-thick $Al_{0.45}Ga_{0.55}N$ barrier. A 12-nm-thick $Al_{0.6}Ga_{0.4}N$ current-blocking layer was then deposited to prevent overflow of the electrons out of the active region. The structure was then completed with a 12-nm-thick *p*-$Al_{0.5}Ga_{0.5}N$ layer with a Mg concentration of 1×10^{19} cm^{-3} (not confirmed) for the *p*-type contact layer.

Electrical and Optical Characterizations: First of all, TLM was used to evaluate the Ohmic contact capability of the proposed CF-based TCEs deposited on both the *p*-GaN and *p*-$Al_{0.5}Ga_{0.5}N$ layers. To fabricate the TLM patterns, mesa isolation was first performed using an inductively coupled plasma etcher. Then, the TLM patterns of the Ni contact pad (100×100 $μm^2$) with varied spacing from 2 μm to 10 μm were defined by photolithography and a development process. In more detail, 80-nm-thick TCE films (ITO, Al_2O_3, ZnO, Ga_2O_3, ZrO_2, SiO_2, ZrN, SiN, and AlN) with isolated mesa structures were deposited on the *p*-GaN and *p*-$Al_{0.5}Ga_{0.5}N$ layers using a radio frequency (RF) magnetron sputtering system in ambient Ar–O_2 (or Ar–N_2) gas at a base pressure of ~2×10^{-7} torr and a working pressure of ~3×10^{-3} torr. The samples were then annealed using rapid thermal processes (RTP) in N_2 gas ambient at 600 °C for 30 s for recrystallization. The Ni top-metal electrode was deposited using an electron beam evaporator, and after that, the lift-off process was performed using acetone. As a result, 18 TLM patterns were transferred onto either *p*-GaN or *p*-$Al_{0.5}Ga_{0.5}N$ wafers of 10×10 mm^2. Figure S3 shows a microscopic image taken for the TLM mask; each mask has 18 TLM patterns at different locations. The electrical characteristics of the contacts were measured using a Keithley 4200 SPA.

Next, to quantitatively evaluate the transmittance of the proposed CF-based TCEs, 80-nm-thick TCE films (ITO, Al_2O_3, ZnO, Ga_2O_3, ZrO_2, SiO_2, ZrN, SiN, and AlN) were deposited on the quartz substrates using the RF sputtering system, after which the samples were then annealed using RTP for recrystallization. Then, we measured the transmittance of the TCE films on the quartz substrates as a function of the wavelength using the *Lambda 35 UV/VIS Spectrometer* with an operating wavelength range from 190 nm to 1100 nm.

Supporting Information

Supporting Information is available from the Wiley Online Library or from the author.

Acknowledgements

This work was supported by the National Research Foundation of Korea (NRF) Grant funded by the Korean government (No. 2011–0028769). The authors would like to thank LG innotek for the supply of UV LED wafers.

Received: May 18, 2013
Revised: September 25, 2013
Published online: November 11, 2013

[1] M. G. Helander, Z. B. Wang, J. Qiu, M. T. Greiner, D. P. Puzzo, Z. W. Liu, Z. H. Lu, *Science* **2011**, *332*, 944.
[2] Y. Yang, Q. Huang, A. W. Metz, J. Ni, S. Jin, T. J. Marks, M. E. Madsen, A. DiVenere, S. T. Ho, *Adv. Mater.* **2004**, *16*, 321.
[3] Y. Galagan, J. E. J. M. Rubingh, R. Andriessen, C. C. Fan, P. W. M. Blom, S. C. Veenstra, J. M. Kroon, *Sol. Energ. Mat. Sol. C* **2011**, *95*, 1339.
[4] H. G. Hong, S. S. Kim, D. Y. Kim, T. Lee, J. O. Song, J. H. Cho, C. Sone, Y. Park, T. Y. Seong, *Appl. Phys. Lett.* **2006**, *88*, 103505.
[5] T. H. Seo, K. J. Lee, T. S. Oh, Y. S. Lee, H. Jeong, A. H. Park, H. Kim, Y. R. Choi, E. K. Suh, T. V. Cuong, V. H. Pham, J. S. Chung, E. J. Kim, *Appl. Phys. Lett.* **2011**, *98*, 251114.
[6] Y. Zhou, C. Fuentes-Hernandez, J. Shim, J. Meyer, A. J. Giordano, H. Li, P. Winget, T. Papadopoulos, H. Cheun, J. Kim, M. Fenoll, A. Dindar, W. Haske, E. Najafabadi, T. M. Khan, H. Sojoudi, S. Barlow, S. Graham, J. L. Brédas, S. R. Marder, A. Kahn, B. Kippelen, *Science* **2012**, *336*, 327.
[7] P. Kuang, J. M. Park, W. Leung, R. C. Mahadevapuram, K. S. Nalwa, T. G. Kim, S. Chaudhary, K. M. Ho, K. Constant, *Adv. Mater.* **2011**, *23*, 2469.
[8] D. J. Chae, D. Y. Kim, T. G. Kim, Y. M. Sung, M. D. Kim, *Appl. Phys. Lett.* **2012**, *100*, 081110.
[9] H. Hirayama, S. Fujikawa, N. Noguchi, J. Norimatsu, T. Takano, K. Tsubaki, N. Kamata, *Phys. Status Solidi A* **2009**, *206*, 1176.
[10] A. Fujioka, T. Misaki, T. Murayama, Y. Narukawa, T. Mukai, *Appl. Phys. Express* **2010**, *3*, 041001.
[11] M. F. Huang, T. H. Lu, *IEEE J. Quantum Electron.* **2006**, *42*, 820.
[12] M. Shatalov, W. Sun, A. Lunev, X. Hu, A. Dobrinsky, Y. Bilenko, J. Yang, M. Shur, R. Gaska, C. Moe, G. Garrett, M. Wraback, *Device Res. Conf.* **2012**, 255.
[13] T. Fujii, Y. Gao, R. Sharma, E. L. Hu, S. P. Den Baars, S. Nakamura, *Appl. Phys. Lett.* **2004**, *84*, 855.
[14] B. J. Kim, C. Lee, Y. Jung, K. H. Baik, M. A. Mastro, J. K. Hite, C. R. Eddy Jr., J. Kim, *Appl. Phys. Lett.* **2011**, *99*, 143101.
[15] T. Mori, K. Nagamatsu, K. Nonaka, K. Takeda, M. Iwaya, S. Kamiyama, H. Amano, I. Akasaki, *Phys. Status Solidi C* **2009**, *6*, 2621.
[16] P. K. Song, Y. Shigesato, I. Yasui, C. W. Ow-Yang, D. C. Paine, *Jpn. J. Appl. Phys.* **1998**, *37*, 1870.
[17] A. Mehonic, S. Cueff, M. Wojdak, S. Hudziak, C. Labbé, R. Rizk, A. J. Kenyon, *Nanotechnology* **2012**, *23*, 455201.
[18] Y. Yang, P. Gao, S. Gaba, T. Chang, X. Pan, W. Lu, *Nat. Commun.* **2012**, *3*, 732.
[19] C. Chen, Y. C. Yang, F. Zeng, F. Pan, *Appl. Phys. Lett.* **2010**, *97*, 083502.
[20] H. D. Kim, H. M. An, E. B. Lee, T. G. Kim, *IEEE Trans. Electron Devices* **2011**, *58*, 3566.
[21] Z. Wei, Y. Kanzawa, K. Arita, Y. Katoh, K. Kawai, S. Muraoka, S. Mitani, S. Fujii, K. Katayama, M. Iijima, T. Mikawa, T. Ninomiya, R. Miyanaga, Y. Kawashima, K. Tsuji, A. Himeno, T. Okada, R. Azuma, K. Shimakawa, H. Sugaya, T. Takagi, R. Yasuhara, K. Horiba, H. Kumigashira, M. Oshima, *IEDM* **2008**, 1
[22] T. Ninomiya, T. Takagi, Z. Wei, S. Muraoka, R. Yasuhara, K. Katayama, Y. Ikeda, K. Kawai, Y. Kato, Y. Kawashima, S. Ito, T. Mikawa, K. Shimakawa, K. Aono, *VLSI Technol.* **2012**, 73.
[23] K. Jung, H. Seo, Y. Kim, H. Im, *Appl. Phys. Lett.* **2007**, *90*, 052104.
[24] H. D. Kim, H. M. An, T. G. Kim, *IEEE Trans. Electron Devices* **2012**, *59*, 2302.
[25] H. H. Berger, *Solid-State Electron.* **1972**, *15*, 145.
[26] H. Murrmann, D. Widmann, *IEEE Trans. Electron Devices* **1969**, *16*, 1022.
[27] H. H. Berger, *J. Electrochem. Soc.* **1972**, *119*, 507.
[28] Y. C. Lin, S. J. Chang, Y. K. Su, T. Y. Tsai, C. S. Chang, S. C. Shei, C. W. Kuo, S. C. Chen, *Solid-State Electron.* **2003**, *47*, 849.
[29] Y. C. Lin, S. J. Chang, Y. K. Su, T. Y. Tsai, C. S. Chang, S. C. Shei, S. J. Hsu, C. H. Liu, U. H. Liaw, S. C. Chen, B. R. Huang, *IEEE Photonics Technol. Lett.* **2002**, *14*, 1668.
[30] W. H. Lee, D. J. Chae, D. Y. Kim, T. G. Kim, *IEEE J. Quantum Electron.* **2011**, *47*, 1277.

© 2013 WILEY-VCH Verlag GmbH & Co. KGaA, Weinheim